Minimum energy and the end of the inspiral in the post-Newtonian approximation

Miriam Cabero,* Alex B. Nielsen, and Andrew P. Lundgren
Max Planck Institute for Gravitational Physics (Albert Einstein Institute),
Callinstrasse 38, D-30167 Hannover, Germany and
Leibniz Universität Hannover, Welfengarten 1-A, D-30167 Hannover, Germany
(Dated: February 10, 2016)

The early inspiral phase of a compact binary coalescence is well modelled by the post-Newtonian (PN) approximation to the orbital energy and gravitational wave flux. The transition from the inspiral phase to the plunge can be defined by the minimum energy circular orbit (MECO). In the extreme mass ratio limit, up to the highest PN order known, the PN energy equals the energy of the exact Kerr solution. However, for comparable mass systems the MECO of the PN energy does not exist when bodies have large spins. By including the exact Kerr limit and recently published post-Newtonian terms we extract a well-defined minimum of the orbital energy beyond which the plunge or merger occurs. We study the hybrid condition for a number of cases of both black hole and neutron stars and compare to other commonly employed definitions. Our method can be used for any known order of the post-Newtonian series and enables the MECO condition to be used to define the end of the inspiral phase for highly spinning, comparable mass systems.

I. INTRODUCTION

Compact objects are the end result of the evolution of massive stars. Neutron stars and black-hole candidates have been observed in close binary systems with massive-star companions. Theoretical models of the evolution of binary systems [1] predict the supernova explosion of the companion star to form a second compact object. If the system survives the explosion, the outcome is a compact binary. Observations of double neutron stars confirmed the existence of compact binaries and allowed further investigations on their formation [2, 3]. Compact binaries with black-hole components have not been observed electromagnetically, but are promising sources of gravitational waves. With the second generation of ground-based gravitational-wave detectors [4–6], gravitational-wave astronomy will open a new window to our understanding of the universe.

Neutron stars are very challenging to describe physically, since not much is known about their equation of state. Black holes, however, are purely geometrical objects and can be described without the complicated physics of matter. The Schwarzschild and the Kerr solutions to Einstein's equations describe the spacetime around a static, spherically symmetric black hole and a stationary, axisymmetric black hole, respectively. The geodesic equations provide information about the trajectory of a test-mass in these spacetimes. Obtaining the circular timelike geodesics in the equatorial plane reduces to a problem of one-dimensional motion in an effective potential V_{eff} [7, 8]. The extrema of this effective potential define the existence of stable and unstable circular orbits. The innermost stable circular orbit (ISCO) is defined by the minimum of V_{eff}.

Black holes are most readily detected through their gravitational interaction with matter. A well known example, Cygnus X-1, consists of a binary system formed by a black-hole candidate and a blue supergiant variable star. Its detection was possible thanks to the X-ray emission of the accretion disk formed by the stellar wind of the star. Relativistic models of thin accretion disks around black holes [9, 10] assume that the inner edge of the disk coincides with the Kerr ISCO. The gas spirals rapidly into the black hole after reaching the ISCO, and therefore the gas density beyond that point is virtually zero. A description of the system by test-mass dynamics is meaningful only when considering the mass of the accretion disk to be much smaller than the mass of the black hole.

If the black hole's binary companion is another compact object of comparable mass, the spacetime of the system is not well described by the Kerr solution. Unfortunately, an exact analytical solution of the two-body problem in general relativity has not been found yet. Post-Newtonian (PN) theory yields an analytical approximation of the motion of compact binaries, under the assumptions of weak gravitational field inside the source and of slow internal motion [11]. Despite these limitations, the PN approximation has proven to be an unexpectedly effective description [12].

The radiation of energy in the form of gravitational waves predicted by Einstein has a decisive effect on the motion of compact binaries. The gravitational-wave emission causes the orbit to gradually shrink, bringing the bodies closer together in a long inspiral phase [13]. Evidence for this effect has been observed for instance in the Hulse-Taylor

binary pulsar [14] and in the "double-pulsar" PSR J0737-3039 [15] with pulsar timing techniques. After the long inspiral, the evolution of compact binary coalescences is followed by a plunge, merger, and ring-down. However, these processes can be interrupted if one of the objects (or both) is a neutron star. Depending on the equation of state, the neutron star can be tidally deformed and even completely disrupted before the plunge phase [16, 17].

In the absence of tidal disruption or magnetic fields, the evolution of the late inspiral phase is mainly driven by gravitational-wave emission. The inspiral phase, where the change in the orbital frequency over each period is negligible (adiabatic regime), can be described via the PN expressions of the energy and flux. Closer orbits have higher orbital velocities and lower orbital energies. In the PN framework, the energy gradually decreases and occasionally reaches a minimum. This minimum determines the end of the inspiral or the range of validity of the PN theory. The orbit at which the energy reaches its minimum value is called the minimum energy circular orbit (MECO), also innermost circular orbit (ICO) in the literature [18]. As we will see, direct application of the minimum energy condition to the known PN energy leads to a MECO that depends sensitively on the PN order and the intrinsic angular momentum (spin) of the black hole.

In the Schwarzschild and Kerr spacetimes, the MECO coincides with the ISCO. However, it has been shown that this statement is not necessarily true in the PN approximation [18, 19]. Blanchet and Iyer [19] computed the ISCO for non-spinning objects in the PN formalism studying the stability of circular orbits against linear perturbations of the equations of motion. They observed that the effect of the PN corrections is to increase the frequency of the ISCO with respect to Schwarzschild (i.e. the ISCO radius is smaller in PN theory than in the Schwarzschild case). A generalisation of their method for spinning objects has been performed by Favata [20].

The end of the inspiral in compact binaries is of great theoretical and practical interest for the two-body problem in general relativity. The dynamics of the coalescence qualitatively change in the transition from the inspiral to the plunge. PN theory breaks down close to the merger due the nature of the approximation. This breakdown is not well-defined, yet a critical issue for gravitational-wave modelling. For instance, waveform templates generated with PN methods require the knowledge of a suitable frequency cutoff. Such templates can be combined with numerical relativity (NR) waveforms at higher frequencies to obtain longer templates that describe the full coalescence. In the past, the exact Schwarzschild ISCO or the PN MECO have been used as frequency cutoff (see [21–23], for instance). However, both approaches have their caveats. On one side, the existence of an ISCO in the full two-body problem is uncertain, and the test-mass limit is not suitable for comparable mass systems. On the other side, the MECO does not always have a finite value.

In this work we study the properties of the MECO in the post-Newtonian theory. We seek to obtain a MECO that exists for any known PN order, any mass-ratio and any value of the spins of the objects. In the extreme mass-ratio inspiral (EMRI) case, the PN approximation is poorly convergent, but one can use the test-mass dynamics of the exact solution [18]. Therefore, we focus here on the case of equal-mass and low mass-ratios, where PN is expected to be accurate. For comparison, we consider mainly two cases: i) a neutron-star black-hole binary (NSBH) of mass-ratio $q = m_{BH}/m_{NS} \simeq 7$, where the spin of the neutron star is set to zero, and ii) an equal-mass binary black-hole (BBH), where both black holes have the same spin. For simplicity, the black-hole spin is aligned or anti-aligned with the orbital angular momentum in both cases.

For these two binary systems, we analyse in section II the dependence of the MECO on the spin and the PN order, and the effects of adding new PN terms published recently. In section III, we use the exact Kerr MECO to analyse the test-mass limit. Following the idea of a hybrid approach introduced in [24], section IV computes a well-defined MECO which has a finite value for any PN order and any spin. Since our result depends only on the mass-ratio and not on the total mass of the binary, it can be also used for systems containing intermediate-mass or supermassive black holes. In section V we introduce the overlap as a measure of the signal-to-noise ratio (SNR) in gravitational-wave searches. Assuming that the end of the inspiral is defined by the MECO proposed in this work, we compute the SNR loss in the Laser Interferometer Gravitational-wave Observatory (LIGO) when using templates that terminate at Schwarzschild ISCO. The sensitivity curves used represent [25] (i) the early runs of the Advanced LIGO generation (which we call early aLIGO), and (ii) the modelled sensitivity of the zero-detuned, high-power design of the mature Advanced LIGO (which we call ZDHP aLIGO). The last two sections are a preparation for future work. Section VI investigates if the integrands used for PN waveform generation are well-posed through the new MECO termination point. This result will be important for faithfulness studies of different waveform models with the new PN terms. Finally, section VII shows the importance of considering tidal effects, such as those published in [26, 27], in NSBH with comparable masses (mass-ratio $q \simeq 2$).

Throughout this paper we use geometrical units $G = c = 1$. We denote the individual masses of the bodies by m_i with $m_1 \geq m_2$, the total mass by $M = m_1 + m_2$, the mass-ratio by $q = m_1/m_2 \geq 1$, and the symmetric mass-ratio by $\eta = m_1 m_2/(m_1 + m_2)^2$. We mostly work with the projection of the dimensionless spin of the black hole on the orbital angular momentum, $\chi_i = \vec{S}_i \cdot \hat{L}/m_i^2$, where $\vec{S}_i$ is the intrinsic angular momentum and $\hat{L}$ is the unit vector along the orbital angular momentum. The projected spin can take values $-1 \leq \chi_i \leq 1$, where positive spins indicate alignment with the orbital angular momentum, and negative spins indicate anti-alignment. In this paper we don't

consider other approximations, such as the effective-one-body (EOB) model [28–30] or Padé approximants [31, 32]. However, in section II we show the frequency peak of the spinning-EOB model calibrated to numerical relativity (SEOBNR peak) for comparison. The SEOBNR peak is the expected value of the instantaneous gravitational-wave frequency at the time when the (2,2) mode amplitude peaks in numerical simulations. Typically, the time at which the common apparent horizon forms in BBH numerical simulations is very close to the time at which the amplitude peaks. Therefore, the SEOBNR peak can be viewed as a proxy for the frequency at which the merger occurs.

II. BEHAVIOUR OF THE MECO AT DIFFERENT POST-NEWTONIAN ORDERS

The PN energy and flux are given as series expansions in the orbital velocity of the binary, v. Terms of order v^{2n} are called nPN terms, where odd nPN orders are those with $n \notin \mathbb{N}$, and even nPN orders have $n \in \mathbb{N}$. Under the assumption of circular orbits, the long and complicated PN expressions get slightly simplified (see appendix B). This is a reasonable approximation for most systems, since the decay of the orbital eccentricity happens much faster than the coalescence of isolated circularly orbiting binaries [33]. For non-spinning systems, the energy in the centre-of-mass frame for circular orbits is known up to 4PN order and the flux up to 3.5PN [34, 35]. The spin corrections to the energy are known up to the 2PN spin-spin [36] and the 3.5PN spin-orbit [37] term. New PN terms have been published recently for systems with spinning objects: the 3PN spin-spin [38], and the 3.5PN spin-cubed [39] terms.

For consistency, the PN energy in the test-mass limit ($m_2 \to 0$) must reproduce the Taylor expansion of the orbital energy of a test-mass in the Kerr spacetime up to the PN order considered. Therefore, one can use the exact Kerr solution for extreme mass-ratios, where the end of the inspiral is given by the Kerr ISCO. The location of the Kerr ISCO in the equatorial plane depends on the spin of the black hole, and in Boyer-Lindquist coordinates is given by [8]

$$r = m \left[3 + Z_2 \mp \sqrt{(3 - Z_1)(3 + Z_1 + 2Z_2)} \right] , \tag{1}$$

$$\text{where} \qquad Z_1 = 1 + \left(1 - \chi^2\right)^{1/3} \left[(1 + \chi)^{1/3} + (1 - \chi)^{1/3} \right] ,$$

$$Z_2 = \sqrt{3\chi^2 + Z_1^2} ,$$

m is the mass of the Kerr black hole, and χ is its projected spin. For spin zero, the Kerr ISCO reduces to the Schwarzschild ISCO, $r = 6m$. The upper sign in equation (1) is for direct orbits (spin of the black hole aligned with the orbital angular momentum), while the lower sign is for retrograde orbits (spin anti-aligned with the orbital angular momentum). For extreme spins ($\chi = \pm 1$), the Kerr ISCO is located at $r = m$ (aligned case) and $r = 9m$ (anti-aligned case). If the mass and spin of the smaller body are not totally neglected, but considered small, self-force calculations provide the corrections due to the effect of the second body [40].

As the mass-ratio decreases, the system does not follow test-mass dynamics of the exact Kerr solution. One must rely on the PN approximation, where the end of the inspiral can be determined through its MECO. Figure 1 shows the orbital velocity of the PN MECO for the two highest orders known until now[1] (i.e. the velocities at which $dE^{PN}/dv = 0$). For comparison, the ISCOs (see appendix A for the relations between the ISCO radius and its orbital velocity) and the SEOBNR peak (obtained from the LSC Algorithm Library Suite [41]) are also shown. As can be seen in the figure, the MECO highly depends on the PN order, and does not exist in certain regions of the parameter space. For high values of the black-hole spins in the BBH case for instance, the MECO does not exist. The NSBH shows the same behaviour for the odd 3.5PN order, while the even 3PN energy reaches a minimum for any value of the black-hole spin. Due to this unstable behaviour, these MECOs are not a suitable definition of the end of the inspiral.

Figure 2 shows the 3.5PN energy for a BBH with different spin values. The orbital energy decreases and reaches a minimum that represents the end of the inspiral (the MECO). What occurs after the minimum is to be discarded physically, since the PN energy cannot describe the dynamics of the system at high frequencies. At high spins, the energy does not show a minimum, and therefore the MECO does not exist. The maximum appearing at $\chi = 0.3$ explains the turn in the "Current 3.5PN MECO" curve in figure 1.

---

[1] Here, the only difference between the 3PN and the 3.5PN orders is the 3.5PN spin-orbit term.
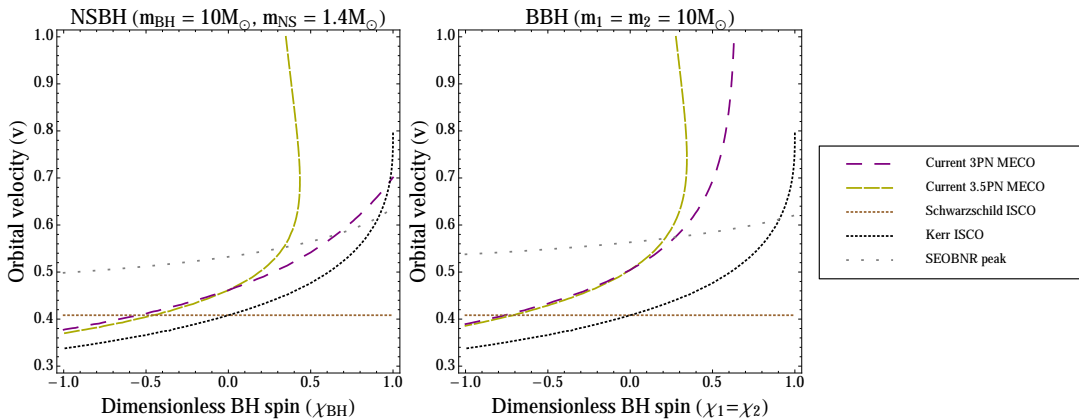
FIG. 1: Different inspiral-cutoffs for NSBH and BBH. Dotted curves represent the Schwarzschild ISCO (constant in spin), the Kerr ISCO (spin-dependent), and the SEOBNR peak. Dashed curves represent the extrema of the PN energy (the MECO and possible maxima of the energy). The neutron-star spin is considered negligible compared to the black-hole spin, and therefore set to zero. The black-hole spins are equal in the BBH case and aligned (positive χ) or anti-aligned (negative χ) with the orbital angular momentum. Except for the 3PN order in the NSBH case, the MECO does not exist in the region of high aligned spins.
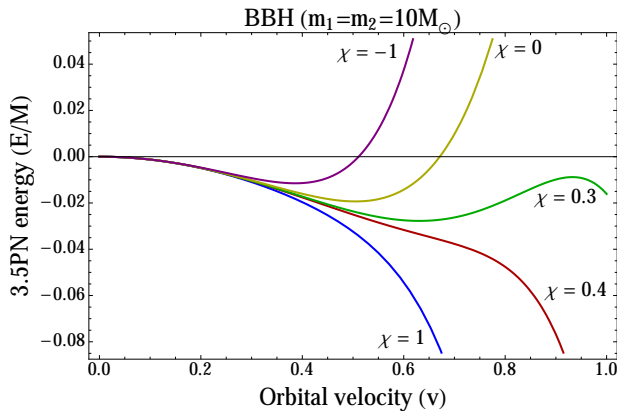

FIG. 2: Current 3.5PN energy as function of the orbital velocity for an equal-mass BBH. The two black holes are considered to have equal spin, $\chi_1 = \chi_2 = \chi$. For spins of $\chi = 0.3$, the energy shows a maximum after the minimum, which explains the turn in the curve of the 3.5PN extrema in figure 1. For high spins ($\chi = 1$ in this plot), the energy does not reach a minimum in the range $0 < v < 1$, and therefore the MECO does not exist at the 3.5PN order.

A. Adding the new PN terms

Due to the absence of a minimum of the energy in certain regions of the parameter space, the current MECO cannot be used as a robust definition of the end of the inspiral. Knowledge of higher order terms in the PN series could lead to a finite well-defined MECO. However, the convergence of the PN series is unknown. In the non-spinning case, it has been shown that the PN series "converges well" in the equal-mass case, but very slowly in the test-mass limit [18]. Here we show how the recent publication of the 4PN non-spinning [35], the 3PN spin-spin [38], and the 3.5PN spin-cubed [39] terms does not provide a better-defined MECO.

The effect of adding the 4PN non-spinning and the 3PN spin-spin terms is shown in figure 3 (the difference due to the 3.5PN spin-cubed term is unnoticeable at the scale of these plots). The change on the 3PN MECO can be seen at the higher aligned-spin values, while the 3.5PN MECO remains nearly unchanged after adding the 3PN spin-spin. The 4PN term has a big effect on the MECO, and behaves similarly to the odd orders in the BBH case. These results show that the addition of new terms does not provide a MECO that is well-defined for any spin value in the equal-mass case.
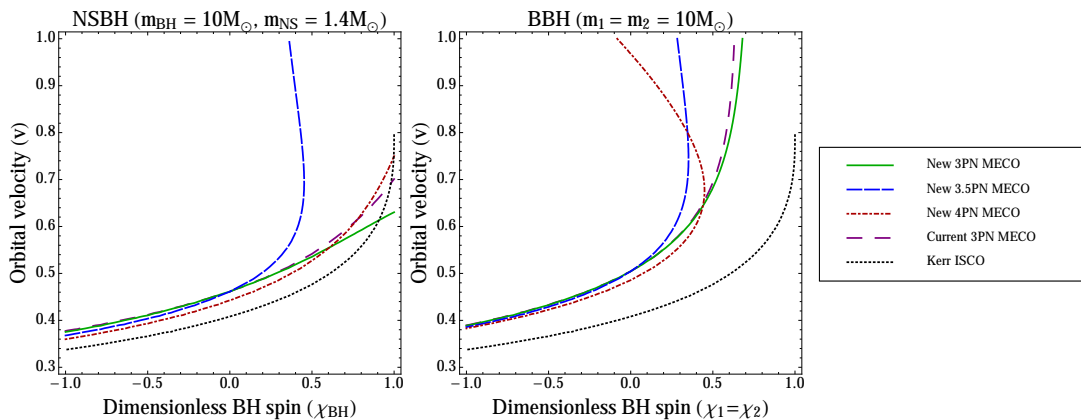
FIG. 3: Effect of the recently published PN terms on the MECO. The Kerr ISCO is shown for comparison. New nPN MECOs include the 3PN spin-spin term and the 4PN non-spinning term. The "Current 3.5PN MECO" is not shown because the difference to the "New 3.5PN MECO" is unnoticeable at the scale of these plots.

III.   PN EXPANSIONS OF THE TEST-MASS LIMIT

The PN approximation is poorly convergent in the test-mass limit, but is expected to be accurate in the comparable-mass regime [18]. Therefore, one would expect the MECO to be well-defined for comparable-mass binaries. However, the previous section has shown that the MECO does not exist for high spins in the equal-mass case. Since this issue has not shown to be mitigated by the addition of higher PN orders, we proceed to analyse the test-mass case, where the PN approximation is already known to fail.

The orbital energy of a test-mass around a Kerr black hole can be given as [20]

$$E^{Kerr} = \left(\frac{1 - 2w + \chi_1 w^{3/2}}{\sqrt{1 - 3w + 2\chi_1 w^{3/2}}} - 1 \right) , \tag{2}$$

where $w = \frac{v^2}{(1-\chi_1 v^3)^{2/3}}$. Here, χ_1 is the projected spin of the black hole, and v is the orbital velocity. For a Kerr black hole, the ISCO coincides with the MECO, which is obtained by solving

$$\frac{dE^{Kerr}}{dv} = 0 . \tag{3}$$

This reduces to obtaining the velocity at which

$$\left(1 - \chi_1 v^3\right) \left[3\chi_1^2 v^4 - \left(1 + 7\chi_1 v^3\right)\left(1 - \chi_1 v^3\right)^{1/3} + 6v^2 \left(1 - \chi_1 v^3\right)^{2/3}\right] = 0 . \tag{4}$$

In the test-mass limit $(m_2 \to 0)$, the PN energy equals the Taylor expansion of the Kerr energy up to the highest PN order known. Expanding equation (2) up to 4PN, we obtain [2]

$$E^{Kerr} \simeq \left. \frac{E^{PN}}{\eta} \right|_{m_2 \to 0} = -\frac{1}{2}v^2 \left[1 - \frac{3}{4}v^2 + \frac{8\chi_1}{3}v^3 - \left(\frac{27}{8} + \chi_1^2\right)v^4 + 8\chi_1 v^5 - \left(\frac{675}{64} + \frac{65\chi_1^2}{18}\right)v^6 \right.$$
$$\left. + 27\chi_1 v^7 - \left(\frac{3969}{128} + \frac{469\chi_1^2}{24}\right)v^8 + \mathcal{O}\left(v^9\right)\right] . \tag{5}$$

Note that we consider also the 4PN spin-spin term $(469\chi_1^2/24)$, even though 3PN is the highest spin-spin term known in the post-Newtonian energy.

A comparison at different PN orders of the exact Kerr MECO (4) to its approximation (given by the minimum of equation (5)) can be seen in figure 4. At higher spins, the MECO of the 4PN expansion for the Kerr energy does

---

[2] The dimensionless spin χ_1 in equation (5) and the PN spin parameter S_1 used in appendix B are related through $\chi_1 = S_1/m_1^2$.

not resemble the MECO of the exact Kerr energy. Therefore, the MECO of the post-Newtonian energy is unlikely to resemble the MECO of its unknown final exact solution, if it exists. Even if one knew the post-Newtonian energy up to 14.5PN, its test-mass part would only converge to the exact known solution up to spins of $\chi \simeq 0.5$, or velocities of $v \simeq 0.45$. Another remarkable feature of the expansion of the Kerr energy is the different behaviour between odd and even PN orders. While even PN orders appear to have a minimum for any value of the spin, odd PN orders do not present extrema for $\chi \gtrsim 0.5$. This behaviour is very similar to what has been seen for the complete PN energy, suggesting that the test-mass part has the strongest effect on the PN MECO.
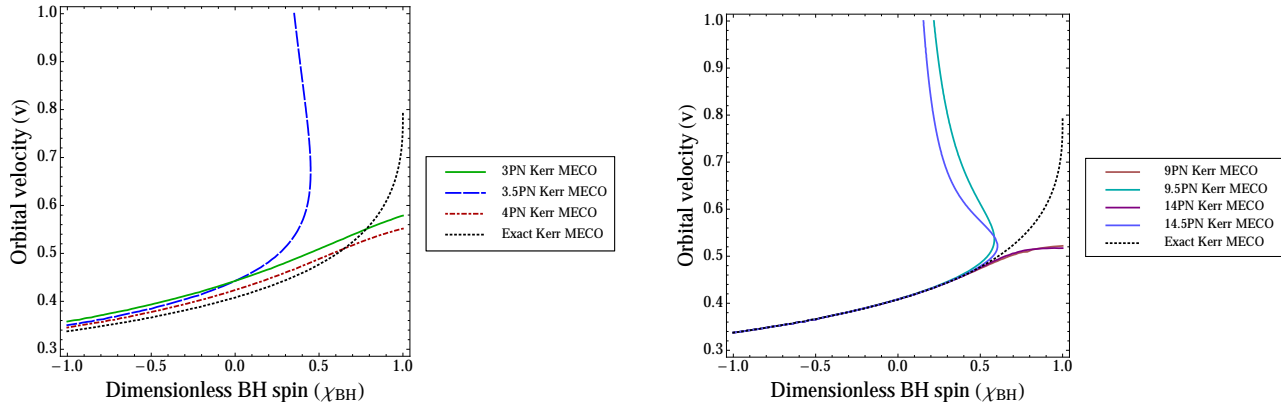

FIG. 4: MECO for a test mass orbiting a Kerr black hole. The dotted curve represents the exact solution. Continuous and dashed lines show different orders of the approximation (5), which are called PN orders for comparison with the PN approximation. The expanded MECO does not approach the exact MECO at high spins, showing a very unstable behaviour for odd PN orders (the upper branch of odd PN orders corresponds actually to a maximum of the energy). Therefore, any attempt to obtain a well-defined MECO for the PN energy at odd orders will fail with the current method.

IV. STABILISATION OF THE MECO

Mathematically, it is unknown if the PN series comes from the Taylor expansion of a family of exact solutions [11]. However, for consistency, its test-mass limit will always equal the expansion of the exact Kerr solution. This expansion has been shown to have a very unstable MECO that converges very slowly to the exact Kerr ISCO. It is necessary to avoid the test-mass expansion in order to obtain a stable MECO which is well-defined for any PN order and any spin value. In this section we use a similar method as in [24], with the addition of the known spin effects.

Consider a hybrid energy given by substituting the test-mass terms of the PN energy for the exact Kerr energy:

$$
\begin{aligned}
E = E^{Kerr} + &\left[\frac{E^{PN}}{\eta} - \left(\frac{E^{PN}}{\eta} \Big|_{m_2 \to 0} \right) \right] \\
= E^{Kerr} - &\frac{1}{2} v^2 \left\{ -\frac{\eta}{12} v^2 + \left(\frac{19}{8}\eta - \frac{\eta^2}{24} \right) v^4 + \left[\left(\frac{34445}{576} - \frac{205\pi^2}{96} \right)\eta - \frac{155}{96}\eta^2 - \frac{35}{5184}\eta^3 \right] v^6 \right. \\
& - \left[\left(\frac{123671}{5760} - \frac{9037\pi^2}{1536} - \frac{1792}{15}\ln 2 - \frac{896}{15}\gamma_E \right)\eta + \left(\frac{498449}{3456} - \frac{3157\pi^2}{576} \right)\eta^2 - \frac{301}{1728}\eta^3 - \frac{77}{31104}\eta^4 - \frac{448}{15}\eta \ln v^2 \right] v^8 \\
& \left. + \left[E_{SO} - \chi_1 \left(\frac{8}{3} v^3 + 8v^5 + 27v^7 \right) \right] + \left[E_{SS}^{2PN} + \chi_1^2 v^4 \right] + \left[E_{SS}^{3PN} + \frac{65}{18}\chi_1^2 v^6 \right] + E_{S^3} \right\},
\end{aligned}
\tag{6}
$$

where E^{Kerr} is the energy given in equation (2) and E_{SO}, E_{SS}^{2PN}, E_{SS}^{3PN} are the spinning terms of the PN energy given in appendix B (recall the relation $S_i = \chi_i m_i^2$). This energy has a minimum for any PN order and for any spin value, as can be seen in figure 5. On systems with high aligned spins, the inspiral ends before reaching the Kerr ISCO (this effect can be seen better on the 3.5PN order than on the even orders). In the absence of higher order spin-orbit terms, one cannot conclude if odd and even orders will tend to approach each other. Nevertheless, due to the stability of this approach at any PN order and any spin, we suggest the use of the hybrid MECO as frequency cutoff in PN waveform generation.

The relative difference between the exact Kerr MECO and this new hybrid MECO at the 3.5PN order is shown in figure 6 as a function of the mass-ratio. The difference becomes more significant for high spins. As the mass-ratio
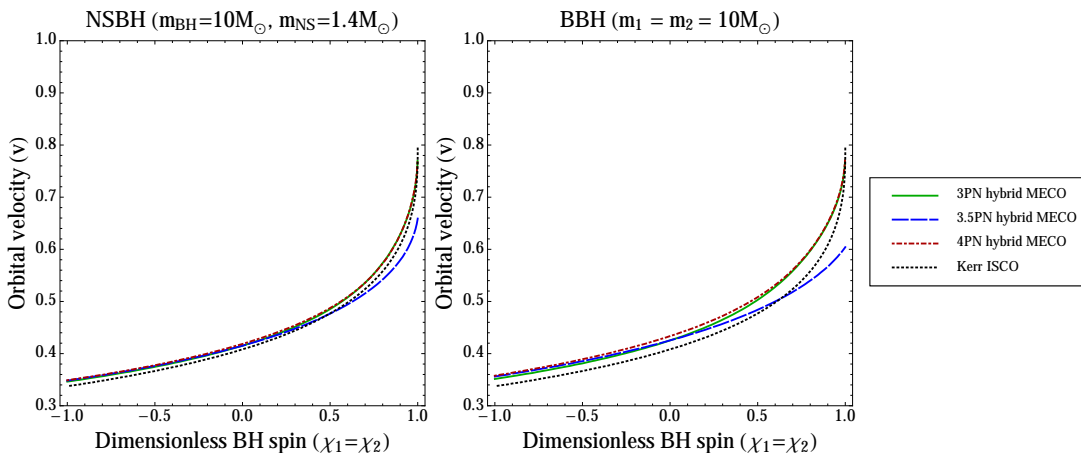
FIG. 5: MECO of the hybrid energy given in equation (6). The dotted curve represents the Kerr ISCO. The deviation from the exact Kerr ISCO depends on the mass-ratio: increasing the mass-ratio leads to higher similarity with the exact Kerr ISCO. There is still a clear difference between odd and even PN orders at high aligned spins. However, the energy always reaches a minimum, suggesting that the hybrid MECO is a better description of the end of the inspiral than the MECO of the pure PN energy.

increases, the difference tends to zero asymptotically. At the extreme spin case ($\chi = 1$), the pathological behaviour of the Kerr energy [8] predominates for the hybrid energy and therefore is not shown in the figure.
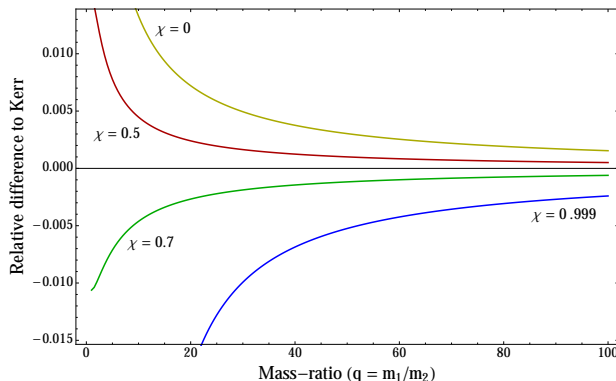

FIG. 6: Relative difference between the hybrid MECO at the 3.5PN order and the exact Kerr MECO $(v_{hybrid} - v_{Kerr})/v_{Kerr}$ for mass-ratios up to $q = 100$. The two black holes are considered to have equal spin, $\chi_1 = \chi_2 = \chi$. Only aligned spins (positive) are shown, because anti-aligned spins behave similarly to the spin zero case.

V. OVERLAP BETWEEN SIGNALS AND TEMPLATES

In the absence of a well-defined MECO, previous PN waveform studies [21, 22] have used the Schwarzschild ISCO or other stopping conditions (like $v = 1$) as cutoff. The Schwarzschild ISCO is valid for systems with negligible spin and high mass-ratio. However, when the objects are spinning, the end of the inspiral depends on the spin of the objects. For anti-aligned spins, the Kerr ISCO is located at lower velocities (i.e. larger separations) than the Schwarzschild ISCO. For aligned spins, the situation is the opposite: the Kerr ISCO is located closer to the black hole than in the non-spinning case. The Schwarzschild and Kerr ISCO coincide at zero spin.

The hybrid MECO proposed in the previous section is also spin-dependent and with similar behaviour to the Kerr ISCO. In this section, we analyse the ability to recover signals that terminate at the hybrid MECO with templates that terminate at the Schwarzschild ISCO. We consider the expected sensitivity curves for the early runs of the advanced LIGO gravitational-wave detectors (early aLIGO) and for the zero-detuned, high-power design of the mature advanced LIGO (ZDHP aLIGO) [25].

Given two waveforms $h_1(t)$ and $h_2(t)$, the inner product is defined by [42, 43]

$$\langle h_1 | h_2 \rangle = 2 \int_0^\infty \frac{\tilde{h}_1^*(f)\tilde{h}_2(f) + \tilde{h}_1(f)\tilde{h}_2^*(f)}{S_n(f)} \, df, \tag{7}$$

where $\tilde{h}_i(f)$ is the Fourier transform of $h_i(t)$ and $*$ indicates complex conjugation. $S_n(f)$ denotes the one-sided power spectral density of the gravitational-wave detector's noise. Since the signal cannot reach arbitrarily high frequencies, the upper frequency cutoff of the integral is the end of the inspiral (the relation between the orbital velocity and the gravitational-wave frequency is given by $v = (\pi M f_{GW})^{1/3}$). The lower limit of the integral will be given by the detector's low-frequency sensitivity, below which the detector is dominated by seismic noise.

The normalised overlap between two waveforms h_1 and h_2 is a fraction of the signal-to-noise ratio (SNR) and is given by [23]

$$\mathcal{O}(h_1, h_2) = \frac{\langle h_1 | h_2 \rangle}{\sqrt{\langle h_1 | h_1 \rangle \langle h_2 | h_2 \rangle}}. \tag{8}$$

We want to analyse if the use of the hybrid MECO can increase the SNR in gravitational-wave searches. This is analogous to computing the overlap between a signal waveform $s(t)$ that terminates at the hybrid MECO frequency (f_M), and a template waveform $h(t)$ that terminates at the Schwarzschild ISCO frequency (f_S). The Fourier domain waveform in the stationary phase approximation is given by [43]

$$\tilde{h}(f) = \mathcal{A} f^{-7/6} e^{i\Psi(f)}, \tag{9}$$

where $\Psi(f)$ is the phase of the Fourier domain waveform and $\mathcal{A}$ its amplitude. With this expression, neglecting all the post-Newtonian corrections to the amplitude and to the phase, the overlap between the signal and the template is given by

$$\mathcal{O}(s, h_t) = \frac{\int_{f_0}^{f_m} \frac{f^{-7/3}}{S_n(f)} \, df}{\sqrt{\left(\int_{f_0}^{f_S} \frac{f^{-7/3}}{S_n(f)} \, df \right) \left(\int_{f_0}^{f_M} \frac{f^{-7/3}}{S_n(f)} \, df \right)}}, \tag{10}$$

where f_0 is the detector's low-frequency sensitivity and $f_m = min(f_M, f_S)$.

Figure 7 shows this overlap as a function of the mass-ratio q. For spins at which the Schwarzschild ISCO and the hybrid MECO coincide, the overlap between the template and the signal is greater than 0.97. For the systems considered, small mass-ratios give a total mass $M < 10 M_\odot$. The frequency of the gravitational wave is inversely proportional to the total mass of the system, $f_{GW} = v^3/(\pi M)$. At such small total masses, the Schwarzschild ISCO and the hybrid MECO have frequencies $f_{GW} \gtrsim 400$Hz. Since the region of greatest sensitivity of the detectors is below 400Hz, changing the waveform cutoff at such high frequencies does not result in a significant gain in the SNR. Therefore low mass-ratios in the figure have overlaps greater than 0.97. However, systems with higher total mass have their inspiral cutoff in the region where the detectors are most sensitive. Using the Schwarzschild ISCO in that region for signals assumed to terminate their inspiral at the hybrid MECO give overlaps as low as 0.4.

VI. APPLICATION TO POST-NEWTONIAN APPROXIMANTS

The PN energy, E^{PN}, and flux, $\mathcal{F}^{PN}$, can be used to compute the evolution of the gravitational-wave phase [22, 23]. From the energy balance equation $dE/dt = -\mathcal{F}$, one can obtain an expression for the time evolution of the orbital velocity v:

$$\frac{dv}{dt} = -\frac{\mathcal{F}(v)}{E'(v)}, \tag{11}$$

where $E'(v) = dE/dv$. Recall that the gravitational wave frequency f_{GW} is related to the orbital velocity by $v = (\pi M f_{GW})^{1/3}$. The gravitational-wave phase is twice the orbital phase $\phi(t)$, which is given by

$$\frac{d\phi}{dt} = \frac{v^3}{M}. \tag{12}$$

The PN approximants are the different methods that are used to solve the energy balance equation and obtain the gravitational-wave phase. In this paper, we focus on the so-called TaylorT4 and TaylorT2 approximants.
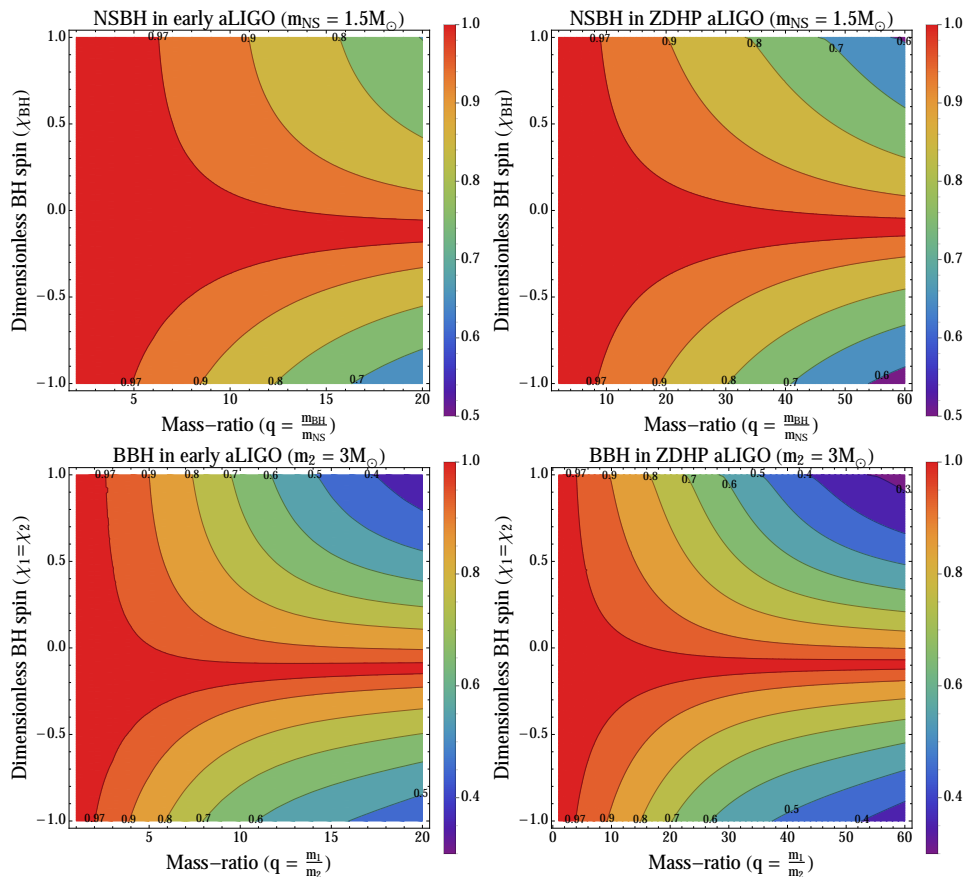
FIG. 7: Overlap between a signal terminating at the Schwarzschild ISCO and a template terminating at the hybrid MECO as a function of the spin of the black hole and the mass-ratio q of the two objects. The mass of one body is fixed: $m_{NS} = 1.5 M_\odot$ in the NSBH case and $m_2 = 3 M_\odot$ in the BBH case. The mass of the other body varies as $m_1 = q m_2$, so the lowest black-hole mass is $m_1 = 3 M_\odot$ in both cases (the lowest mass-ratio in the NSBH case is $q = 2$). For early aLIGO, $f_0 = 30$Hz and q goes up to 20. For ZDHP aLIGO, $f_0 = 10$Hz and q goes up to 60.

The TaylorT4 approximant, proposed in [44], is obtained by expanding the ratio $\mathcal{F}(v)/E'(v)$ to the consistent PN order and then integrating equation (11) numerically. Introducing the result $v(t)$ into equation (12), the phase of the gravitational wave can be integrated.

The TaylorT2 approximant expands to the consistent PN order the ratio $E'(v)/\mathcal{F}(v)$ instead:

$$\frac{dt}{dv} = -\frac{E'(v)}{\mathcal{F}(v)} \,. \tag{13}$$

The phase can then be obtained combining (12) and (13), and integrating

$$\frac{d\phi}{dv} = -\frac{v^3}{M}\frac{E'(v)}{\mathcal{F}(v)} \,. \tag{14}$$

Ideally the phase is integrated up to the MECO frequency in both approximants. However, there are regions of the compact binary parameter space where the MECO does not exist. One wants to avoid integrating beyond the range of validity of the PN approximation and beyond physical values of the velocity. Therefore, further cutoff conditions are imposed [23]: *(i)* the characteristic velocity of the binary must be less than the speed of light ($v \leq 1$), *(ii)* the rate of increase in frequency must not decrease ($dv/dt \geq 0$ for TaylorT4), and *(iii)* analogous to the previous condition, $dt/dv \geq 0$ for TaylorT2. Consequently, the waveform might terminate before reaching the MECO (when it exists) due to these extra cutoff conditions.

The hybrid MECO proposed in section IV exists in any region of the parameter space and is less than $v = 1$. Therefore, the additional condition (i) described above is not required. However, the approximant could still terminate before reaching the hybrid MECO if the cutoff conditions (ii) and (iii) are met. Figure 8 shows the regions of the

parameter space where the integrands become zero before reaching the hybrid MECO at the 3.5PN order[3]. For the TaylorT4 approximant, the $dv/dt = 0$ condition is needed at high aligned spins. On the contrary, the $dt/dv = 0$ condition for the TaylorT2 approximant happens before reaching the hybrid MECO at high anti-aligned spins.
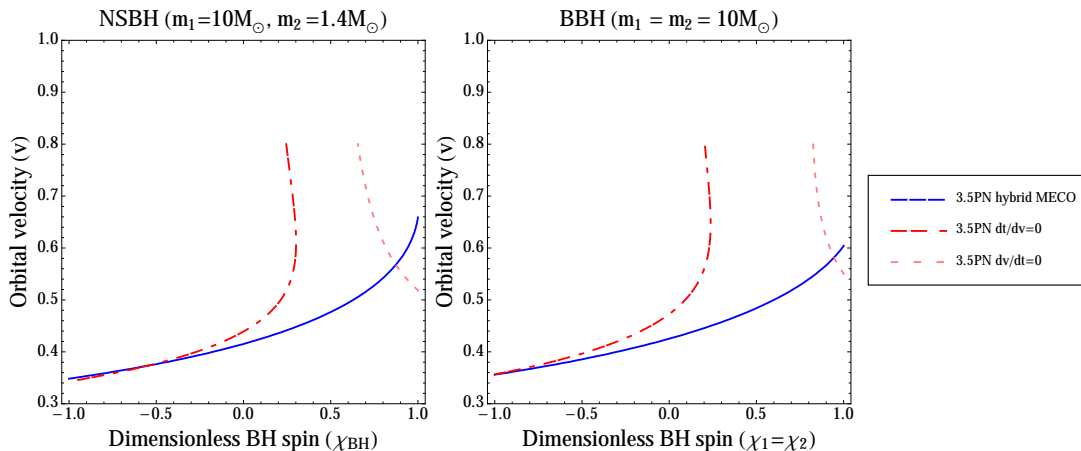

FIG. 8: Hybrid MECO and the integrands cutoffs at the 3.5PN order (with the new 3PN spin-spin term included). TaylorT4 breaks before the hybrid MECO at high aligned spins, and TaylorT2 at high anti-aligned spins.

VII. EFFECT OF THE TIDAL DEFORMATION OF NEUTRON STARS

The dynamics of NSBH binaries are influenced by the tidal deformation of the neutron star when the separation between the two bodies decreases [26, 27, 45, 46]. The magnitude of the deformation depends on the equation of state (EOS) of the neutron star and the mass-ratio between the two objects. For comparable masses, the neutron star may completely disrupt before the plunge into the black hole [45]. In this case, different scenarios such as mass ejection to infinity [45] or the formation of an accretion disk [47] are possible. Such systems are of great astrophysical interest, because they may provide an electromagnetic counterpart to gravitational-wave signals (e.g. short gamma-ray bursts [47]).

An analytical model that accounts for the disruption of the neutron star is more difficult to define. However, some works have computed leading-order terms that describe tidal deformation [26, 27]. Tidal corrections to the PN energy are a Newtonian effect that scale proportional to 5PN order. For a NSBH, where the neutron star is considered the only deformable body[4], these effects are given by [26, 27]

$$E_{tidal} = -\frac{1}{2}\eta v^2 \left[-\frac{9m_1}{m_2}\tilde{\lambda}_2 v^{10} - \frac{11m_1}{2m_2}\left(3 + \frac{2m_2}{M} + \frac{3m_2^2}{M^2}\right)\tilde{\lambda}_2 v^{12} \right] + \mathcal{O}(v^{14})$$

$$\mathcal{F}_{tidal} = \frac{32}{5}\eta^2 v^{10}\left[\left(\frac{18M}{m_2} - 12\right)\tilde{\lambda}_2 v^{10} - \frac{M}{28m_2}\left(704 + 1803\frac{m_2}{M} - 4501\frac{m_2^2}{M^2} + 2170\frac{m_2^3}{M^3}\right)\tilde{\lambda}_2 v^{12}\right] + \mathcal{O}(v^{14}), \quad (15)$$

where $\tilde{\lambda}_2 = \lambda_2(m_2/M)^5$, $\lambda_2 = \frac{2}{3}k_2(R/m_2)^5$ is the dimensionless tidal deformability of the neutron star, k_2 is the Love number of the neutron star, R is its radius, and m_2 is its mass [51, 52].

The tidal correction E_{tidal} contributes positively to the PN energy E^{PN}. Therefore, the orbital velocity at which the energy reaches its minimum will be smaller when the tidal effects are considered. Figure 9 shows the change on the hybrid MECO due to the tidal deformation of the neutron star. The effect of this deformation is to hasten the end of the inspiral, especially for large aligned black-hole spins. This effect depends strongly on the EOS and the mass-ratio, starting to become noticeable for deformability parameters $\lambda_2 > 50$ at mass-ratio $q = 2$ and as high as $\lambda_2 > 5000$ at mass-ratio $q = 10$. Only in the aligned black-hole spin case the tidal effects can be observed in the end of the inspiral, with small black holes preferred.

---

[3] The 4PN order cannot be used for waveform generation because the corresponding flux term is unknown yet.

[4] The deformability of black holes and the value of their Love numbers is still ongoing work [48–50].
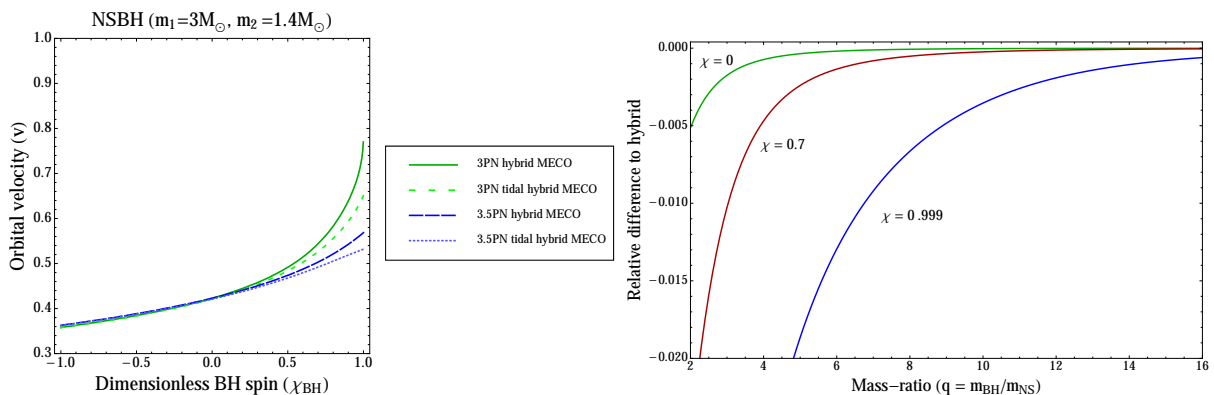
FIG. 9: Change on the hybrid MECO due to the tidal effects given in equation (15). The equation of state of the neutron star considered is AP4, which gives a radius $R = 11.5$ km and a dimensionless tidal deformability $\lambda_2 = 269.75$ [41]. *Left:* qualitative effect of the tidal terms on the hybrid MECO for a mass-ratio $q \simeq 2$. This system is chosen because it clearly shows the effect at high spins. However, total disruption of the neutron star might happen before the MECO is reached. *Right:* relative difference between the hybrid MECO at the 3.5PN order with and without tidal terms $(v_{tidal} - v_{hybrid})/v_{hybrid}$ for mass-ratios up to 16. The mass of the neutron star is fixed to $m_{NS} = 1.4 M_\odot$.

The tidal terms in equation (15) do not account for complete disruption. If the neutron star disrupts, the dynamics of the system change and the tidal hybrid MECO does not suffice to describe the end of the inspiral. Numerical simulations of NSBH [53, 54] provide a better understanding of the disruption mechanism. Based on the resulting numerical waveforms, studies of the end of the inspiral due to the disruption of the neutron star have been performed in [17]. It is important to determine whether disruption occurs before the tidal hybrid MECO, so we also include systems that potentially tidally disrupt in figure 9.

VIII. CONCLUSION

We constructed a hybrid MECO by combining the information of post-Newtonian theory with the exact Kerr solution, and showed that it can be used for binary systems with arbitrary component spins. In combination with NR simulations and full inspiral-merger-ringdown waveform models, this simple analytical approximation gives a more complete understanding of the dynamics of compact binaries.

Unlike the pure PN MECO, which does not exist for large component spins, the hybrid MECO is well-defined for any known PN order in the whole parameter space. This feature is very important for gravitational-wave searches, where component spins have a significant effect. Furthermore, the hybrid MECO is well-defined for equal-mass binaries and, by construction, reduces to the Kerr ISCO in the test-mass limit. This suggests that this approach can be used for arbitrary mass-ratios. In addition, the method we propose can be easily updated when new post-Newtonian terms become available by adding the non test-mass part of the new terms to the hybrid energy. Finite-mass corrections can also be introduced in the hybrid energy, as we have shown, for instance, with the tidal effects of neutron stars.

Several future applications of this cutoff condition can be considered. One application is the usage of the hybrid MECO in faithfulness studies of different PN waveforms with different frequency cutoffs. We showed that with the standard Fourier domain waveform in the stationary phase approximation and the designed sensitivity of advanced LIGO detectors, the overlap can vary by more than 50% if the hybrid MECO is used against the spin-independent Schwarzschild ISCO. Therefore, previous studies that used the Schwarzschild ISCO or a fixed frequency as cutoff can be updated with our approach. Another application is to extend the hybrid MECO to include spin-precessing terms. In this paper we have worked only with component spins aligned with the orbital angular momentum. However, the behaviour of the MECO could vary significantly for precessing systems. Finally, direct comparisons between the tidal hybrid MECO and the cutoff obtained from total tidal disruption models may provide more information about the end of the inspiral in systems with neutron stars.

Appendix A: Relations between parameters

The Kerr ISCO location given in equation (1) is coordinate dependent. It is customary to express the orbital radius in terms of the orbital velocity, obtaining a gauge-invariant ISCO which is independent of the total mass of the system. We use the coordinate angular velocity given in [8, 20] to approximate a relation between the separation of the two objects r and the PN orbital velocity v at the leading order:

$$\frac{M}{r} = \frac{v^2}{(1 - \chi v^3)^{2/3}} \, . \tag{A1}$$

At zero spin, this relation reduces to $v = \sqrt{M/r}$, which gives a velocity of $v = 1/\sqrt{6} \simeq 0.41$ for the Schwarzschild ISCO. For extreme spins ($a = m$), the Kerr ISCO corresponds to velocities of $v \simeq 0.79$ (aligned case) and $v \simeq 0.34$ (antialigned case). The frequency of the gravitational wave is related to the orbital velocity through $v = (\pi M f_{GW})^{1/3}$.

One can use the phase of the gravitational wave to compute the number of cycles between different terminations. The number of gravitational-wave cycles $\mathcal{N}$ between the velocities v_1 and v_2 can be given by

$$\mathcal{N} = \frac{\phi^{GW}(v_2) - \phi^{GW}(v_1)}{2\pi} \, , \tag{A2}$$

where $\phi^{GW}(v)$ is the gravitational-wave phase (twice the orbital phase). The gravitational-wave phase as function of the frequency can be obtained from equation (3.11) in [42] (or the orbital phase as function of the velocity from equations (318) and (3.8a) in [34] and [22], respectively). At the leading order, the gravitational-wave phase is independent of the spin and is given by

$$\phi^{GW}(v) = -\frac{1}{16v^5\eta} \, . \tag{A3}$$

Between the minimum and the maximum velocity of the Kerr ISCO, the number of gravitational-wave cycles for an equal-mass binary ($\eta = 0.25$) is $\mathcal{N} \simeq 8.6$, and $\mathcal{N} \simeq 43.1$ for a binary with $\eta = 0.05$. In the bandwidth of a gravitational-wave detector with lower frequency cutoff at $f_0 = 30 Hz$, the gravitational wave of an equal-mass BBH with total mass $M = 20 M_\odot$ will be visible from $v_1 \simeq 0.21$ and will show $\mathcal{N} \simeq 97.3$ cycles when it reaches $v_2 \simeq 0.79$. For this gravitational wave, the 8.6 cycles between the Kerr ISCO velocities represent the 8.8% of the complete inspiral gravitational wave.

Appendix B: Post-Newtonian energy and energy flux

The derivation of the different terms of the post-Newtonian energy and energy flux in the centre-of-mass frame can be found in the literature [34–39]. Here we want to collect in one place all the terms that we have used in this paper. Since the orbits of compact binaries are expected to circularise by the time they become visible with current gravitational-wave detectors, we restrict ourselves to the expressions for circular orbits. The different terms in the energy and the flux are:

$$E^{PN} = -\frac{1}{2}\eta v^2 \left[E_{NS} + E_{SO} + E_{SS} + E_{S^3} \right] , \tag{B1}$$

$$\mathcal{F}^{PN} = \frac{32}{5}\eta^2 v^{10} \left[\mathcal{F}_{NS} + \mathcal{F}_{SO} + \mathcal{F}_{SS} + \mathcal{F}_{S^3} \right] , \tag{B2}$$

where NS are the non-spinning terms, SO the spin-orbit terms, SS the spin-spin terms, and S^3 the spin-cubed terms. The individual masses of the bodies are the denoted m_1 and m_2, $M = m_1 + m_2$ is the total mass of the binary, and $\eta = m_1 m_2/m^2$ is the symmetric mass ratio.

The non-spinning energy terms are known up to 4PN [22, 34]

$$\begin{aligned}
E_{NS} = 1 &- \left(\frac{3}{4} + \frac{\eta}{12}\right) v^2 - \left(\frac{27}{8} - \frac{19}{8}\eta + \frac{\eta^2}{24}\right) v^4 - \left[\frac{675}{64} - \left(\frac{34445}{576} - \frac{205\pi^2}{96}\right)\eta + \frac{155}{96}\eta^2 + \frac{35}{5184}\eta^3\right] v^6 \\
&- \left[\frac{3969}{128} + \left(\frac{123671}{5760} - \frac{9037\pi^2}{1536} - \frac{1792}{15}\ln 2 - \frac{896}{15}\gamma_E\right)\eta + \left(\frac{498449}{3456} - \frac{3157\pi^2}{576}\right)\eta^2 \right. \\
&\left. - \frac{301}{1728}\eta^3 - \frac{77}{31104}\eta^4 - \frac{448}{15}\eta\ln v^2\right] v^8 + \mathcal{O}\left(v^{10}\right) ,
\end{aligned} \tag{B3}$$

where γ_E is the Euler constant.

For the spinning terms, we define the variables

$$\mathbf{S} = \mathbf{S}_1 + \mathbf{S}_2 , \qquad \mathbf{\Sigma} = M\left(\frac{\mathbf{S}_2}{m_2} - \frac{\mathbf{S}_1}{m_1}\right) ,$$

$$S_L = \frac{\mathbf{S} \cdot \mathbf{L}}{M^2} , \qquad \Sigma_L = \frac{\mathbf{\Sigma} \cdot \mathbf{L}}{M^2} ,$$

where $\mathbf{S}_1$ and $\mathbf{S}_2$ are the individual vector spins of the objects, and $\mathbf{L}$ is the unit vector pointing in the direction of the orbital angular momentum. We will also use $S_{1L} = \mathbf{S}_1 \cdot \mathbf{L}$ and $S_{2L} = \mathbf{S}_2 \cdot \mathbf{L}$.

The spin-orbit terms are known up to 3.5PN [37]

$$E_{SO} = \left(\frac{14}{3}S_L + 2\delta\Sigma_L\right) v^3 + \left[\left(11 - \frac{61}{9}\eta\right) S_L + \left(3 - \frac{10}{3}\eta\right)\delta\Sigma_L\right] v^5$$
$$+ \left[\left(\frac{135}{4} - \frac{367}{4}\eta + \frac{29}{12}\eta^2\right) S_L + \left(\frac{27}{4} - 39\eta + \frac{5}{4}\eta^2\right)\delta\Sigma_L\right] v^7 + \mathcal{O}\left(v^8\right) , \tag{B4}$$

where $\delta = (m_1 - m_2)/m$.

The 2PN spin-spin term is given by [36, 38]

$$E_{SS}^{2PN} = \left[-S_L^2\left(q_+ + 2\right) + S_L\Sigma_L\left(-\delta q_+ - 2\delta + q_-\right) + \Sigma_L^2\left(\left(\frac{\delta q_-}{2} - \frac{q_+}{2}\right) + \eta\left(q_+ + 2\right)\right)\right] v^4 , \tag{B5}$$

where $q_+ = q_1 + q_2$ and $q_- = q_1 - q_2$. The constants q_i are the quadrupole terms and represent the distortion of the bodies due to their spins (see [55] for more details). For black holes, $q_i = 1$. For neutron stars, the quadrupole term takes values between $q_i \simeq 4 - 8$, depending on the equation of state.

The 3PN spin-spin term, published recently for spin-aligned orbits [38], is given by

$$E_{SS}^{3PN} = \left\{ S_L^2\left[-\left(\frac{5\delta q_-}{3} + \frac{25 q_+}{6} - \frac{50}{9}\right) + \eta\left(\frac{5 q_+}{6} + \frac{5}{3}\right)\right]\right.$$
$$+ S_L\Sigma_L\left[-\left(\frac{5\delta q_+}{2} - \frac{25\delta}{3} - \frac{5 q_-}{2}\right) + \eta\left(\frac{5\delta q_+}{6} + \frac{5\delta}{3} + \frac{35 q_-}{6}\right)\right]$$
$$\left. + \Sigma_L^2\left[\left(\frac{5\delta q_-}{4} - \frac{5 q_+}{4} + 5\right) + \eta\left(\frac{5\delta q_-}{4} + \frac{5 q_+}{4} - 10\right) - \eta^2\left(\frac{5 q_+}{6} + \frac{5}{3}\right)\right] \right\} v^6 . \tag{B6}$$

The spin-cubed term, published recently for spin-aligned orbits [39], is given by

$$E_{S^3} = \left\{ S_L^3\left(2 q_+ + 4\lambda_+ - 20\right) + S_L^2\Sigma_L\left(2\delta q_+ + 6\delta\lambda_+ - 32\delta + 4 q_- - 6\lambda_-\right)\right.$$
$$+ S_L\Sigma_L^2\left[5\delta q_- - 6\delta\lambda_- - 5 q_+ + 6\lambda_+ - 12 - \eta\left(2 q_+ + 12\lambda_+ - 68\right)\right]$$
$$\left. + \Sigma_L^3\left[-3\delta q_+ + 2\delta\lambda_+ + 3 q_- - 2\lambda_- - \eta\left(2\delta\lambda_+ - 12\delta + 6 q_- - 6\lambda_-\right)\right] \right\} v^7 , \tag{B7}$$

where $\lambda_+ = \lambda_1 + \lambda_2$ and $\lambda_- = \lambda_1 - \lambda_2$. The constants λ_i are the octupole terms and characterise the deformation of the bodies due to their spins [39]. For black holes, $\lambda_i = q_i = 1$. For neutron stars, the value of λ_i is yet unknown.

The non-spinning energy flux terms are known up to 3.5PN [22, 34]

$$\mathcal{F}_{NS} = 1 - \left(\frac{1247}{336} + \frac{35}{12}\eta\right) v^2 + 4\pi v^3 - \left(\frac{44711}{9072} - \frac{9721}{504}\eta - \frac{65}{18}\eta^2\right) v^4 - \left(\frac{8191}{672} + \frac{538}{24}\eta\right)\pi v^5$$
$$+ \left[\frac{6643739519}{69854400} + \frac{16\pi^2}{3} - \frac{1712}{105}\gamma_E - \left(\frac{134543}{7776} - \frac{41\pi^2}{48}\right)\eta - \frac{94403}{3024}\eta^2 - \frac{775}{324}\eta^3 - \frac{856}{105}\ln\left[16 v^2\right]\right] v^6$$
$$- \left(\frac{16285}{504} - \frac{214745}{1728}\eta - \frac{193385}{3024}\eta^2\right)\pi v^7 + \mathcal{O}\left(v^8\right) , \tag{B8}$$

where γ_E is the Euler constant.

The spin-orbit terms are known up to 3.5PN [37]

$$\mathcal{F}_{SO} = -\left(4S_L + \frac{5}{4}\delta\Sigma_L\right)v^3 + \left[\left(-\frac{9}{2} + \frac{272}{9}\eta\right)S_L + \left(-\frac{13}{16} + \frac{43}{4}\eta\right)\delta\Sigma_L\right]v^5$$
$$- \left(16\pi S_L + \frac{31\pi}{6}\delta\Sigma_L\right)v^6$$
$$+ \left[\left(\frac{476645}{6804} + \frac{6172}{189}\eta - \frac{2810}{27}\eta^2\right)S_L + \left(\frac{9535}{336} + \frac{1849}{126}\eta - \frac{1501}{36}\eta^2\right)\delta\Sigma_L\right]v^7 + \mathcal{O}\left(v^8\right), \qquad (B9)$$

where $\delta = (m_1 - m_2)/m$.

The 2PN spin-spin term is given by [36, 38]

$$\mathcal{F}_{SS}^{2PN} = \left[S_L^2\left(2q_+ + 4\right) + S_L\Sigma_L\left(2\delta q_+ + 4\delta - 2q_-\right) + \Sigma_L^2\left(\left(-\delta q_- + q_+ + \frac{1}{16}\right) + \eta\left(-2q_+ - 4\right)\right)\right]v^4, \qquad (B10)$$

where $q_+ = q_1 + q_2$ and $q_- = q_1 - q_2$.

The 3PN spin-spin term, published recently for spin-aligned orbits [38], is given by

$$\mathcal{F}_{SS}^{3PN} = \left\{ S_L^2\left[\left(\frac{41\delta q_-}{16} - \frac{271q_+}{112} - \frac{5239}{504}\right) - \eta\left(\frac{43q_+}{4} + \frac{43}{2}\right)\right]\right.$$
$$+ S_L\Sigma_L\left[-\left(\frac{279\delta q_+}{56} + \frac{817\delta}{56} - \frac{279q_-}{56}\right) - \eta\left(\frac{43\delta q_+}{4} + \frac{43\delta}{2} + \frac{q_-}{2}\right)\right]$$
$$\left. + \Sigma_L^2\left[\left(\frac{279\delta q_-}{112} - \frac{279q_+}{112} - \frac{25}{8}\right) + \eta\left(\frac{45\delta q_-}{16} + \frac{243q_+}{112} + \frac{344}{21}\right) + \eta^2\left(\frac{43q_+}{4} + \frac{43}{2}\right)\right]\right\}v^6. \qquad (B11)$$

The spin-cubed term, published recently for spin-aligned orbits [39], is given by

$$\mathcal{F}_{S^3} = \left\{ -S_L^3\left(\frac{16q_+}{3} + 4\lambda_+ - \frac{40}{3}\right) - S_L^2\Sigma_L\left(\frac{35\delta q_+}{6} + 6\delta\lambda_+ - \frac{73\delta}{3} + \frac{3q_-}{4} - 6\lambda_-\right)\right.$$
$$- S_L\Sigma_L^2\left[\frac{35\delta q_-}{12} - 6\delta\lambda_- - \frac{35q_+}{12} + 6\lambda_+ - \frac{32}{3} - \eta\left(\frac{22q_+}{3} + 12\lambda_+ - \frac{172}{3}\right)\right]$$
$$\left. + \Sigma_L^3\left[\frac{67\delta q_+}{24} - 2\delta\lambda_+ - \frac{\delta}{8} - \frac{67q_-}{24} + 2\lambda_- + \eta\left(\frac{\delta q_+}{2} + 2\delta\lambda_+ - 11\delta + \frac{61q_-}{12} - 6\lambda_-\right)\right]\right\}v^7, \qquad (B12)$$

where $\lambda_+ = \lambda_1 + \lambda_2$ and $\lambda_- = \lambda_1 - \lambda_2$.

[1] K. A. Postnov and L. R. Yungelson, Living Reviews in Relativity **17** (2014).
[2] K. Belczyinski, V. Kalogera, and T. Bulik, The Astrophysical Journal **572**, 407 (2002).
[3] V. Kalogera, K. Belczyinski, C. Kim, R. O'Shaughnessy, and B. Willems, Physics Reports **442**, 75 (2007).
[4] The LIGO Scientific Collaboration, Classical and Quantum Gravity **32**, 074001 (2015).
[5] The Virgo Collaboration, Classical and Quantum Gravity **32**, 024001 (2015).
[6] The KAGRA Collaboration, Phys. Rev. D **88**, 043007 (2013).
[7] R. M. Wald, *General Relativity* (The University of Chicago Press, 1984).
[8] J. M. Bardeen, W. H. Press, and S. A. Teukolsky, The Astrophysical Journal **178**, 347 (1972).
[9] I. D. Novikov and K. S. Thorne, in *Black holes (les astres occlus)*, edited by C. DeWitt and B. S. DeWitt (Gordon and Breach Science publishers, 1973).
[10] J. E. McClintock, R. Narayan, S. W. Davis, L. Gou, A. Kulkarni, J. A. Orosz, R. F. Penna, R. A. Remillard, and J. F. Steiner, Classical and Quantum Gravity **28**, 114009 (2011).
[11] L. Blanchet, in *Mass and motion in General Relativity*, edited by L. Blanchet, A. Spallicci, and B. Whiting (Springer, 2011), vol. 162 of *Fundamental Theories of Physics*.
[12] C. M. Will, Proceedings of the National Academy of Sciences **108**, 5938 (2011).
[13] P. C. Peters and J. Mathews, Phys. Rev. **131**, 435 (1963).
[14] J. M. Weisberg and J. H. Taylor, ASP Conf. Ser. **328**, 25 (2004).
[15] M. Burgay, N. D'Amico, A. Possenti, R. N. Manchester, A. G. Lyne, B. C. Joshi, M. A. McLaughlin, M. Kramer, J. M. Sarkissian, F. Camilo, et al., Nature **426**, 531 (2003).
[16] F. Pannarale, L. Rezzolla, F. Ohme, and J. S. Read, Phys. Rev. D **84**, 104017 (2011).

[17] F. Pannarale, E. Berti, K. Kyotoku, B. D. Lackey, and M. Shibata, Phys. Rev. D **92**, 081504 (2015).

[18] L. Blanchet, Physical Review D **65**, 124009 (2002).

[19] L. Blanchet and B. R. Iyer, Classical and Quantum Gravity **20**, 755 (2003).

[20] M. Favata, Physical Review D **83**, 024028 (2011).

[21] T. Dal Canton, A. H. Nitz, A. P. Lundgren, A. B. Nielsen, D. A. Brown, T. Dent, I. W. Harry, B. Krishnan, A. J. Miller, K. Wette, et al., Physical Review D **90**, 082004 (2014).

[22] A. Buonanno, B. R. Iyer, E. Ochsner, Y. Pan, and B. S. Sathyaprakash, Physical Review D **80**, 084043 (2009).

[23] A. H. Nitz, A. Lundgren, D. A. Brown, E. Ochsner, D. Keppel, and I. W. Harry, Physical Review D **88**, 124039 (2013).

[24] L. E. Kidder, C. M. Will, and A. G. Wiseman, Phys. Rev. D **47**, 3281 (1993).

[25] L. Barsotti and P. Fritschel, Technical note LIGO-T1200307-v4, LIGO (2014).

[26] J. Vines, É. É. Flanagan, and T. Hinderer, Physical Review D **83**, 084051 (2011).

[27] L. Wade, J. D. E. Creighton, E. Ochsner, B. D. Lackey, B. F. Farr, T. B. Littenberg, and V. Raymond, Physical Review D **89**, 103012 (2014).

[28] T. Damour and A. Buonanno, Phys. Rev. D **59**, 084006 (1999).

[29] A. Buonanno, Y. Pan, H. P. Pfeiffer, M. A. Scheel, L. T. Buchman, and L. E. Kidder, Phys. Rev. D **79**, 124028 (2009).

[30] Y. Pan, A. Buonanno, L. T. Buchman, T. Chu, L. E. Kidder, H. P. Pfeiffer, and M. A. Scheel, Phys. Rev. D **81**, 084041 (2010).

[31] T. Damour, B. R. Iyer, and B. S. Sathyaprakash, Phys. Rev. D **57**, 885 (1998).

[32] T. Damour, B. R. Iyer, and B. S. Sathyaprakash, Phys. Rev. D **62**, 084036 (2000).

[33] P. C. Peters, Phys. Rev. **136**, B1224 (1964).

[34] L. Blanchet, Living Reviews in Relativity **17** (2014).

[35] D. Bini and T. Damour, Physical Review D **87**, 121501 (2013).

[36] B. Mikóczi, M. Vasúth, and L. Á. Gergely, Physical Review D **71**, 124043 (2005).

[37] A. Bohé, S. Marsat, and L. Blanchet, Classical and Quantum Gravity **30**, 135009 (2013).

[38] A. Bohé, G. Faye, S. Marsat, and E. K. Porter, Classical and Quantum Gravity **32**, 195010 (2015).

[39] S. Marsat, Classical and Quantum Gravity **32**, 085008 (2015).

[40] E. Poisson, A. Pound, and I. Vega, Living Reviews in Relativity **14** (2011).

[41] *LSC Algorithm Library Suite*, URL https://www.lsc-group.phys.uwm.edu/daswg/projects/lalsuite.html.

[42] C. Cutler and É. É. Flanagan, Phys. Rev. D **49**, 2658 (1994).

[43] E. Poisson and C. M. Will, Phys. Rev. D **52**, 848 (1995).

[44] A. Buonanno, Y. Chen, and M. Vallisneri, Physical Review D **67**, 104025 (2003).

[45] J. M. Lattimer and D. N. Schramm, The Astrophysical Journal **210**, 549 (1976).

[46] M. Vallisneri, Physical Review Letters **84**, 3519 (2000).

[47] E. Nakar, Physics Reports **442**, 166 (2007).

[48] T. Damour and O. M. Lecian, Physical Review D **80** (2009).

[49] M. Cabero and B. Krishnan, Classical and Quantum Gravity **32**, 045009 (2015).

[50] E. Poisson, Physical Review D **91** (2015).

[51] T. Hinderer, The Astrophysical Journal **677**, 1216 (2008).

[52] T. Damour and A. Nagar, Phys. Rev. D **80**, 084035 (2009).

[53] M. Shibata, K. Kyotoku, T. Yamamoto, and K. Taniguchi, Phys. Rev. D **79**, 044030 (2009).

[54] K. Kyotoku, H. Okawa, M. Shibata, and K. Taniguchi, Phys. Rev. D **84**, 64018 (2011).

[55] E. Poisson, Physical Review D **57**, 5287 (1998).